Journal of Medicinal Chemistry

Article

pubs.acs.org/jmc

Function of the D-Alanine:D-Alanine Ligase Lid Loop: A Molecular Modeling and Bioactivity Study

Martina Hrast,[†,§] Blaž Vehar,[‡,§] Samo Turk,[†] Janez Konc,[‡] Stanislav Gobec,*[,†] and Dušanka Janežič*[,‡]

[†]Faculty of Pharmacy, University of Ljubljana, Aškerčeva 7, SI-1000 Ljubljana, Slovenia

[‡]National Institute of Chemistry, Hajdrihova 19, SI-1000 Ljubljana, Slovenia

S *Supporting Information*

ABSTRACT: D-Alanine:D-alanine ligase (Ddl) is an essential ATP-dependent bacterial enzyme involved in peptidoglycan biosynthesis. Discovery of Ddl inhibitors not competitive with ATP has proven to be difficult because the Ddl bimolecular D-alanine binding pocket is very restricted, as is accessibility to the active site for larger molecules in the catalytically active closed conformation of Ddl. A molecular dynamics study of the opening and closing of the Ddl lid loop informs future structure-based design efforts that allow for the flexibility of Ddl. A virtual screen on generated enzyme conformations yielded some hit inhibitors whose bioactivity was determined.

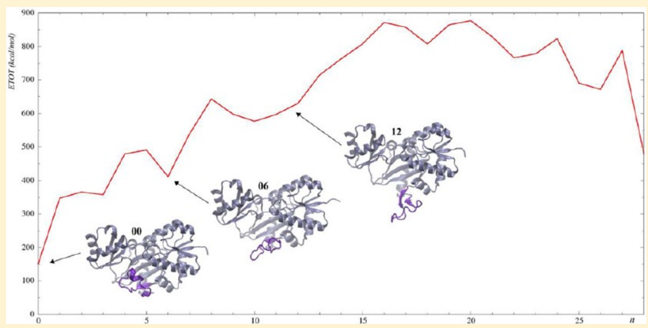

■ INTRODUCTION

D-Alanine:D-alanine ligase (Ddl) is an ATP-dependent bacterial enzyme involved in intracellular stages of peptidoglycan biosynthesis. Its product, D-alanyl-D-alanine (Figure 1), is the terminal dipeptide of UDP-*N*-acetylmuramoyl pentapeptide, the peptidoglycan monomer unit assembled in the Mur-ligase enzyme cascade. Subsequently, this D-alanyl-D-alanine terminus is involved in transpeptidation, the cross-linking of growing peptidoglycan chains. Disruption of D-alanyl-D-alanine biosynthesis can lead to weakening of the cell wall and bacterial cell lysis. Accordingly, Ddl is considered an attractive target for antibacterial drug discovery.[1−5]

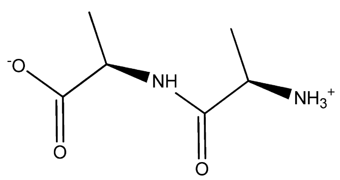

Figure 1. D-Alanyl-D-alanine.

The only inhibitor of Ddl in therapeutic use is D-cycloserine, a rigid cyclic derivative of D-alanine (Figure 2). Like Ddl, D-cycloserine competitively inhibits alanine racemase, the enzyme responsible for the production of D-alanine from L-alanine, abundant in bacterial cells.[6,7] D-Cycloserine is known to be neurotoxic, and its therapeutic use is nowadays limited to second line treatment of tuberculosis.[8]

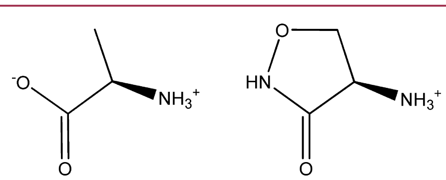

Figure 2. D-Alanine (left) and D-cycloserine (right).

Two isoforms of D-alanine:D-alanine ligase, DdlA and DdlB, exist in both *Escherichia coli* and *Salmonella typhimurium*. DdlA and DdlB share 35% sequence identity and express similar substrate specificity and susceptibility to known inhibitors. Our research focused on the more extensively studied DdlB isoform.[9,10]

DdlB belongs to the ATP-grasp superfamily of proteins with conserved ATP-binding folds.[11] The central cavity of the catalytically active conformation of DdlB includes an ATP binding pocket located between the central and the C-terminal domain and a bimolecular D-alanine binding pocket located between the N-terminal and the C-terminal domain (Figure 3).[12] There are two Mg^{2+} ions at the center of the cavity; they represent a binding anchor for the phosphate moiety of ATP.[13,14] It is unclear whether the magnesium ions originate in the enzyme itself or migrate into the binding pocket together with the incoming ATP molecule.

The C-terminal domain of DdlB contains a flexible lid loop, shown in Figure 3, that covers the central cavity of the protein. Two antiparallel β-strands (residues 201−205 and 221−225) form the stem of the lid loop. Residues 206−220 constitute the head of the lid loop and include a two-turn α-helix (residues 212−217).[15] The proximity of hinge residues 200 and 226 qualifies the Ddl lid loop as an ω-loop protein motif.[16]

During its catalytic cycle, DdlB undergoes two major conformational changes. Rotation of the central domain toward

Received: April 25, 2012
Published: July 17, 2012

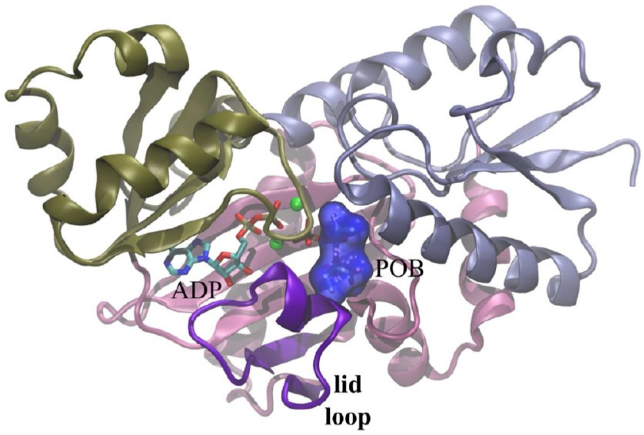

Figure 3. DdlB in cartoon representation. The N-terminal, central, and C-terminal domains are colored ice blue, olive, and mauve, respectively. The lid loop within the C-terminal domain is colored violet. The bimolecular D-alanine binding pocket is shown as a blue transparent surface. ADP and 2-[(1-aminoethyl)phosphate phosphinoyloxy]butyric acid (POB), the crystallized ligands in 1IOV, are shown as sticks. The two phosphate-binding Mg^{2+} ions are shown as green spheres.

the C-terminal domain coincides with the binding of ATP, while the swing motion of the lid loop effectively closes the central cavity upon binding of the D-alanines.[17] Since our goal in this work was to discover ligands that bind specifically to the D-alanine binding pocket, the central domain rotation was overlooked and we focused solely on the motion of the lid loop.

We previously performed virtual screening for inhibitors of DdlB and found that none of our discovered inhibitors bound exclusively to the D-alanine binding pocket; all also interacted with residues in the ATP binding pocket.[18,19] The main reasons for this behavior are the small cavity volume of the D-alanine binding pocket and its limited accessibility to molecules larger than D-alanine. Docking molecules of druglike size into the D-alanine binding pocket alone results in very few hits, mainly because the candidates are unable to fit in in the absence of an open access route from the protein surface. Additionally, a 2D similarity search using D-cycloserine as a query yielded no active compounds; the data are presented in the Supporting Information. This further confirms the importance of complex approaches to finding new inhibitors of DdlB.

In this article we explore the molecular dynamics of the enzyme to identify physically plausible conformations of DdlB with an open access route to the active site. An open conformation of DdlB was generated through comparative modeling. The transition path between the open and the closed conformation was simulated with targeted molecular dynamics and a path optimization simulation. Three of the predicted pathway conformations of DdlB were then used as targets in a double multiconformational virtual screening experiment. The bioactivity of predicted inhibitors was experimentally verified in an enzyme inhibition assay.[20] Reported calculations were limited to those that were essential for identification of novel active compounds.

■ RESULTS AND DISCUSSION

Preparation of DdlB Starting Conformations for Molecular Dynamics Simulations. The native *E. coli* DdlB (PDB entry 1IOV)[12] was chosen as the closed conformation template for our studies. The apo form of the *Thermus caldophilus* Ddl (PDB entry 2FB9),[14] which shares 40% sequence identity with 1IOV, was used to build comparative models of *E. coli* DdlB with an exposed lid loop. The highest ranked of 90 comparative models that were produced was selected as the DdlB open conformation template for further manipulation (Figure 4).

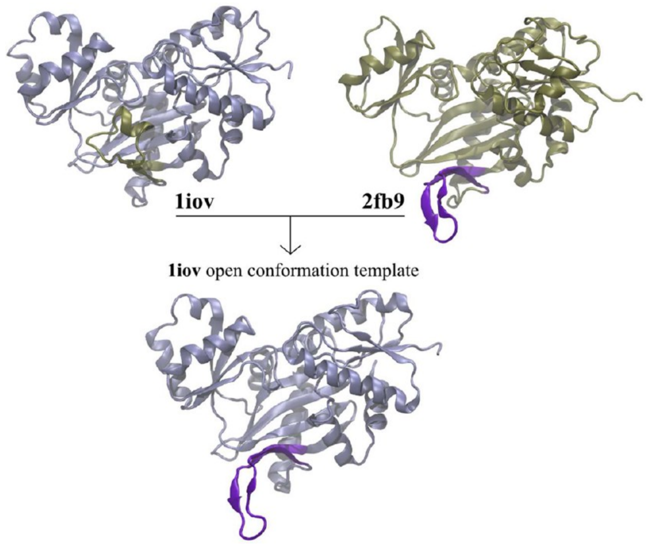

Figure 4. Front views of the closed conformation of *E. coli* DdlB (top left), the open conformation of *T. caldophilus* DdlB (top right), and our comparative model of *E. coli* DdlB (bottom) composed from both. The exposed lid loop is colored violet. The parts of the crystal structures that were not used in the calculation of the comparative model are colored olive.

The protein chain of 1IOV was stripped of all non-protein species except for two phosphate-binding magnesium ions present in its active site. The protein chain of the open conformation template was overlaid onto 1IOV, and the coordinates of the Mg^{2+} ions were copied into the open conformation. Then both enzyme structures were optimized with the CHARMM program for molecular dynamics simulations,[21] as described in the Experimental Section. The structures of the closed 1IOV conformation and its fully open counterpart that were obtained through this process were used as bookend conformations for the simulation of the motion of the lid loop.

Simulation of the DdlB Lid Loop Motion. To obtain plausible intermediate DdlB structures between the fully closed and the fully open conformations, a targeted molecular dynamics (TMD) simulation[22] was performed, resulting in 40 conformations of DdlB ranging from fully closed (1IOV_0) to fully open (1IOV_39). Five of these are shown in Figure 5. Since the last third of the TMD simulation consisted entirely of a spatial rearrangement of a fully exposed lid loop in the solvent, the last 10 conformations (1IOV_30 to 1IOV_39) were omitted from subsequent simulations.

An off-path/replica path simulation[23,24] was then run to optimize the transition pathway, as has been described previously.[25,26] Conformations 1IOV_0 to 1IOV_29 from TMD, thoroughly minimized in CHARMM with the ABNR method, were used as reference points for the off-path simulation. After 314 ps of the off-path simulation, the conformations were minimized with the SD method and labeled 00 (closed) through 29 (open). They were checked for

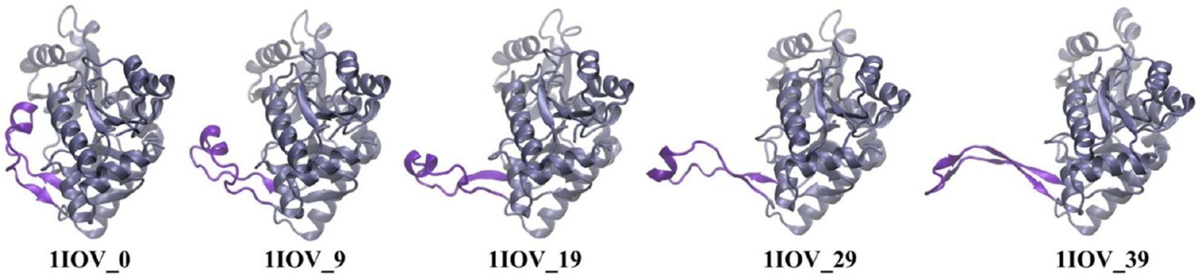

Figure 5. Side views of five DdlB conformations from the TMD-predicted lid loop motion pathway. The lid loop is colored violet.

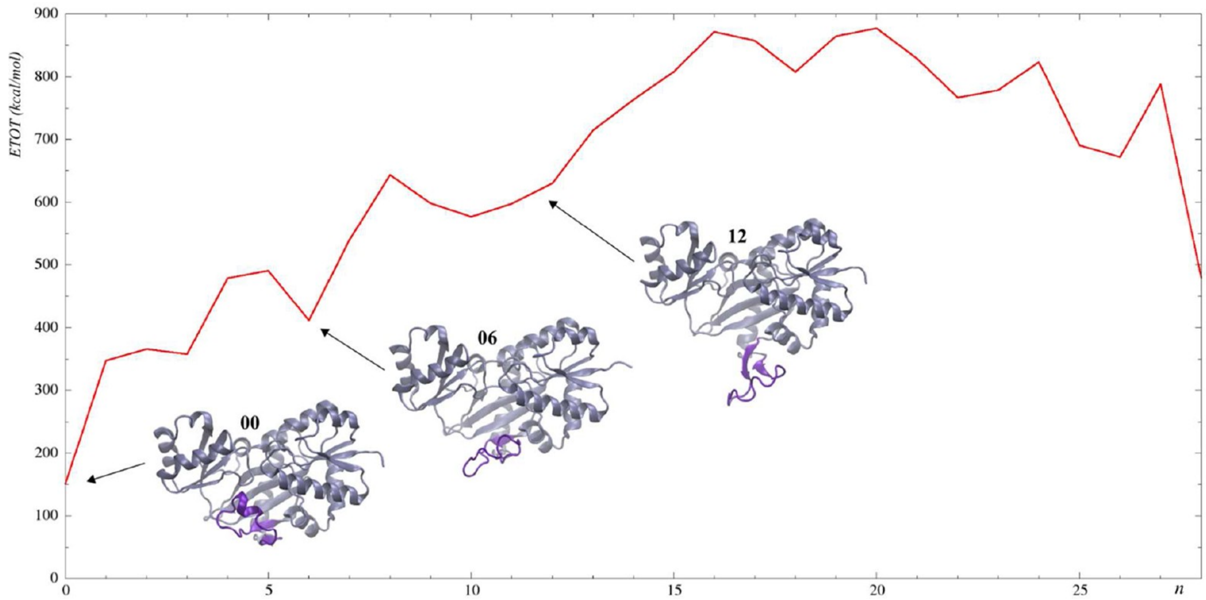

Figure 6. Energy profile for the replica path potential of mean force, calculated as the work it takes for the system to move from simulation plane to simulation plane along the transition pathway (ETOT in CHARMM). *n* is the number of each consecutive pair of conformations. Shown in cartoon form are conformations 00, 06, and 12, inhabiting local minima of the energy profile.

equal rms distances between each consecutive pair, as shown in Supporting Information. The potential of mean force for the transition pathway was calculated from the simulation data (Figure 6). As conformations inhabiting local minima on the transition pathway, 00, 06, and 12 were respectively selected as the closed, semiclosed, and semiopen conformations of DdlB suitable for further use.

Lid Loop Interactions along the Transition Pathway. In the catalytically active closed conformation 00 of *E. coli* DdlB (Figure 7, top left), the lid loop is in contact with several other parts of the enzyme: residues Tyr210 and Tyr216 form bonds with the C-terminal domain β-sheet; Phe209, Tyr212, and Lys215 interact with the central domain; Tyr212 and Tyr216 point toward the N-terminal domain; Tyr216 and Asp219 interact with the C-terminal domain loop connecting residues 277 and 281 which is close to the N-terminal domain. Our simulation results propose a distinct order in which these interactions should be nullified during the opening of the lid loop.

The first casualties of the lid loop motion are its bonds to the C-terminal β-sheet. The β-strand stem of the lid loop bulges toward the solvent, enlarging the central cavity volume. The head of the lid loop, although slightly rearranged, maintains most of its original interactions (Figure 7, top right). This bulging process occurs between conformations 01 and 03 in our MD simulation.

Between conformations 03 and 06, the bonds to the central and the N-terminal domain also gradually disappear. The longest and strongest interacting loop residue among these, Lys215, migrates away from first Ser150 and then Ser151, while the head of the lid loop rotates away from the enzyme body. In conformation 06 (Figure 7, bottom left), the central cavity of DdlB is readily accessible to druglike molecules.

The interaction of Asp219 with the C-terminal domain loop 277−281 persists until conformation 12 (Figure 7, bottom right). Even in some later conformations, side chains of residues 218−221 remain in the vicinity of His280, implying possibilities of transient interactions. In conformations beyond 12 in our simulations, the lid loop is completely exposed to solvent molecules and the calculated conformations are less reliable. The conformations in which the lid loop residues interact only with the solvent are irrelevant for the mechanism of DdlB lid loop motion and any consequences of this motion.

Structure-Based Virtual Screening. To demonstrate one of the possible uses of our simulation results, a virtual screen was performed using conformations 00, 06, and 12 to find small molecules that potentially bind into the D-alanine binding pocket of the Ddl active site.

To allow for selective binding into the D-alanine binding pocket, an ATP molecule was inserted into each enzyme conformation (Figure 8) using the position of ADP from the crystal structure 1IOV as a template. This was achieved in

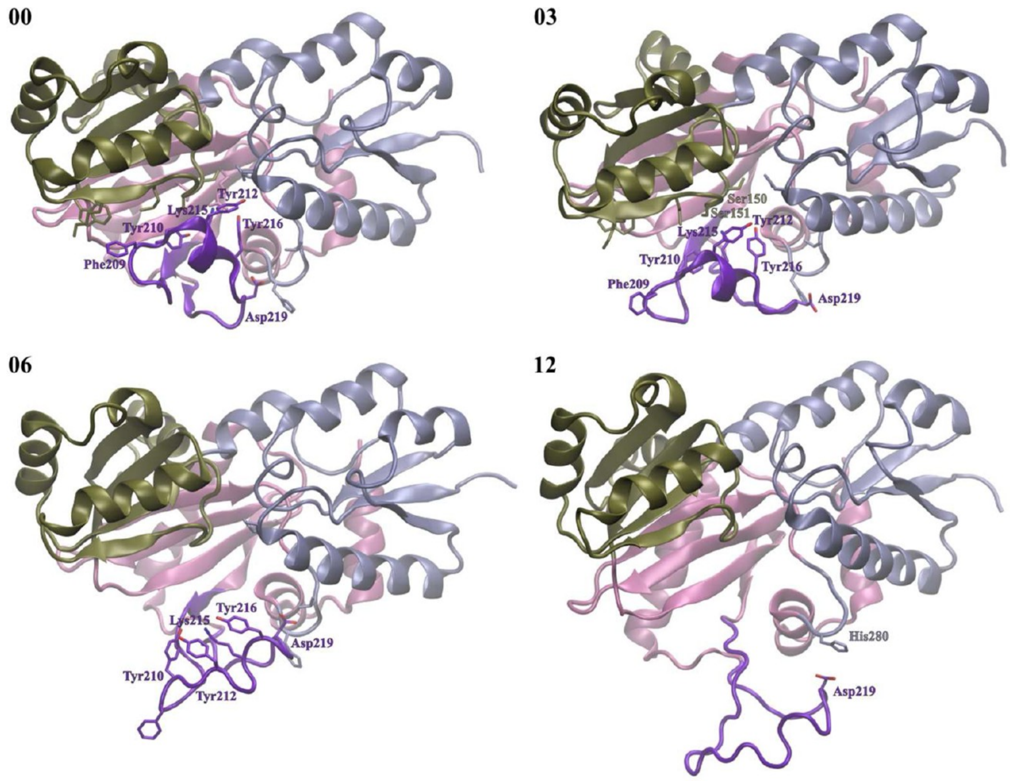

Figure 7. Lid loop interactions in DdlB conformations 00, 03, 06, and 12. The N-terminal domain and its neighboring loop are colored ice blue. The central domain is colored olive. The lid loop is colored violet, and the rest of the C-terminal domain is colored mauve. Side chains of interacting residues are shown as sticks.

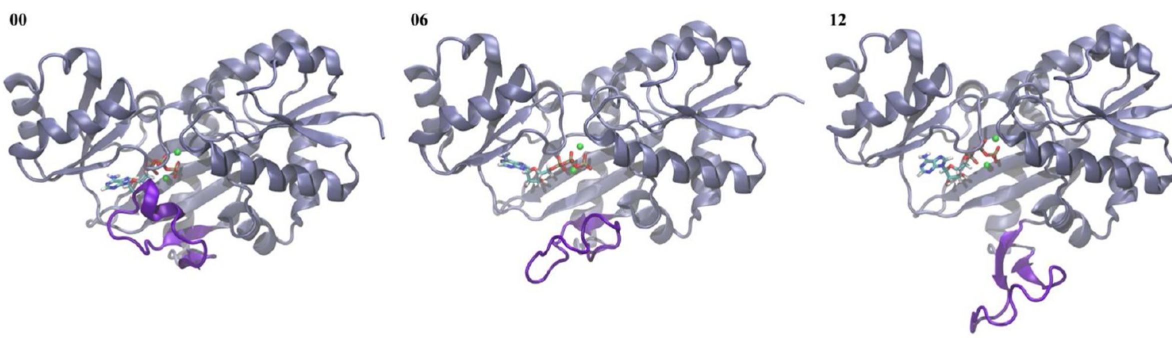

Figure 8. Cartoon representations of ATP-containing DdlB conformations 00 (closed), 06 (semiclosed), and 12 (semiopen) used in docking runs. ATP is shown as sticks. Mg^{2+} ions are shown as green spheres. The lid loop is colored violet.

CHARMM with its rmsd-dependent tool for orienting molecule coordinates. Next, the ATP-containing closed, semiclosed, and semiopen conformations were quickly minimized to avoid steric clashes and other unfavorable contacts with ATP. Minimized conformations were used as enzyme targets in docking runs. With ATP present in the active site of the enzyme, only the bimolecular D-alanine binding pocket and the lid loop residues were available to interact with incoming ligands. This meant that potential docking hits were selectively D-alanine competitive.

To obtain a ligand library, compounds from suppliers Asinex, ChemBridge, Maybridge, and the U.S. National Cancer Institute were selected and downloaded from the ZINC database,[27] yielding 1.9 million compounds. A filtering procedure was applied to provide a more focused compound bank containing roughly 146 000 structures. The choice of filter descriptors was based loosely on fragment based rules to allow for thorough conformational searching, better ligand efficiency, and faster screening. Compounds with reactive functional groups were also removed to eliminate potentially toxic compounds and to reduce the possibility of nonspecific inhibition.

Two software tools, FlexX[28] and Fred,[29] were used to perform separate structure-based virtual screens of the filtered compound library on three different ATP-containing forms of DdlB (the closed, semiclosed, and semiopen enzyme conformations), yielding six scoring lists. A consensus score was calculated by adding scoring ranks from all six individual scoring lists. To avoid the grouping of very similar compounds at the top of the consensus score list, a hierarchical clustering was performed with the in-house program PyScoreClust to produce a less redundant top-100 list of compounds. These compounds were assayed for enzyme inhibition. When the

Table 1. The Most Potent Compounds from the Enzyme Inhibition Assay

compd	cluster number	ZINC code	structure	MW	% RA at 500 μM (unless noted otherwise)	IC_{50} (μM)
1	17	ZINC08536193	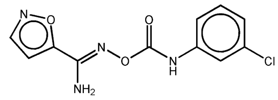	280.671	48	378
2	45	ZINC18142224	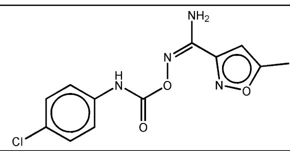	295.706	61	656
3	43	ZINC01868219	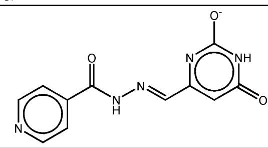	259.225	62	nd[a]
4	96	ZINC01586033	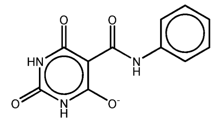	247.210	63	611
5	63	STK046256 (homologue of ZINC06420593)	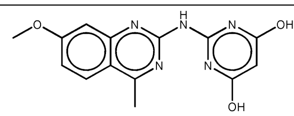	299.290	70 (at 250 μM)	nd[a]
6	24	ZINC04351284	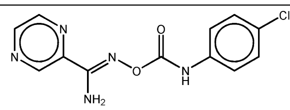	291.698	77	nd[a]
7	20	ZINC05092259	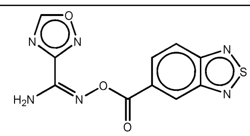	290.264	78	nd[a]

[a]Not determined because of low solubility.

lowest scoring compound in a cluster was unavailable, another member of the cluster was assayed.

The two docking programs used in this research employ either flexible searching of conformational space or multi-conformational rigid shape complementarity to predict binding of ligands to their targets. These differences, along with the effects of docking into different enzyme conformations and subsequent clustering of the consensus score list, explain the relatively high scores of compounds in the final top-100 list, given in the Supporting Information.

Enzyme Inhibition Assay. The top 100 compounds from the clustered consensus list were tested for activity against DdlB from *E. coli*. Seven of the tested compounds, shown in Table 1, lowered the activity of DdlB to 80% or less at 500 or 250 μM. Attempts were made to determine IC_{50} values for all active compounds. Because of the low solubility of the compounds, which were mostly insoluble at concentrations higher than 600 μM, we were able to measure inhibitory activities at only four different concentrations (200, 300, 400, and 500 μM). Consequently, approximate IC_{50} values could be estimated for inhibitors **1**, **2**, and **4** and are presented in Table 1. The solubility of the other four active compounds was too low to allow estimation of their IC_{50} values. The IC_{50} of D-cycloserine, determined in a previous study using equal assay conditions,[30] was 314 μM, in the same order of magnitude as IC_{50} values of **1**, **2**, and **4**.

For compound **1**, the most potent inhibitor of this series, further kinetic analysis was attempted. Similarly as in IC_{50} determination, only four concentrations were used because of the low solubility of the compound at higher concentrations. The data obtained gave a best estimate of K_i at 326 ± 89 μM and revealed that compound **1** is a D-alanine competitive inhibitor. This indicates that **1** binds to the D-alanine binding pocket and that the observed inhibition is not a result of nonspecific interactions.

The active compounds from Table 1 all have nitrogen- and/or oxygen-rich linkers of various lengths connecting two aromatic moieties. Compounds **1**, **2**, and **6** all have a carbamoyloxycarboximidamide linker between aromatic rings and have activities that are inversely proportional to the size of their aromatic groups. Compound **7** has a similar but slightly shorter linker. In compounds **3**, **4**, and **5**, one of the aromatic groups is a barbituric acid derivative. All seven compounds were verified for identity and purity, as described in the Experimental Section.

While inhibitors of DdlB with better activities have been described previously, our compounds are predicted to bind preferentially to the bimolecular D-alanine binding pocket and are therefore worth exploring further in search of selective non ATP-competitive binding partners of DdlB. The proposed binding modes of the inhibitors from Table 1 with a short analysis and comparison to a transition state analogue inhibitor are presented in the Supporting Information.

■ CONCLUSIONS

The motion of the DdlB lid loop, studied with a combination of comparative modeling, targeted molecular dynamics, and a parallel off-path/replica path simulation method, was described in terms of the order of interactions that weaken and break during the loop opening.

A double virtual screen was performed on three conformations of DdlB. Following the consensus scoring of six sets of screening results and hierarchical clustering of the top 10 000 compounds, the representatives of the highest ranked 100 clusters were tested for inhibition of *E. coli* DdlB in an enzyme inhibition assay. Four compounds lowered the enzyme activity by at least one-third at 250 or 500 μM. These compounds are predicted to bind selectively to the bimolecular D-alanine binding pocket, unlike the inhibitors from our previous research.

The closed, semiclosed, and semiopen conformations of DdlB described in this study are useful templates in view of the flexible nature of this bacterial ligase and could prove to be beneficial to the ongoing discovery of new antimicrobial agents.

To our best knowledge, only a few compounds are known to inhibit Ddl. With the exception of D-cycloserine, most of them have much higher molecular masses and belong to very different structural classes. Therefore, we believe that the compounds presented in this paper represent an important starting point for further optimization and development.

■ EXPERIMENTAL SECTION

I. Molecular Modeling. *Computer Hardware.* The computational procedures were carried out on three separate workstations and the VRANA-11 parallel computer cluster.[31,32] The FlexX workstation has four dual core AMD Opteron 2.0 GHz processors and is running Fedora Linux. The OpenEye workstation has two quad core Intel Xeon 2.2 GHz processors and is running Arch Linux. The workstation used for Modeller, CHARMM, and PyScoreClust has two quad core Intel Xeon 2.4 GHz processors and is running Ubuntu Linux. The VRANA-11 cluster consists of 26 computers, each with two quad core Intel Xeon 2.0 GHz processors and running Gentoo Linux.

Preparation of the DdlB Open Conformation Template. A comparative model of the open conformation of *E. coli* DdlB was built with the Modeller 9v6 software[33] from two crystal structures: the native DdlB from *E. coli* (1IOV, lid loop closed) and the apo form of Ddl from *T. caldophilus* (2FB9, lid loop exposed). Both crystal structures were downloaded as text files from the RCSB PDB Web site.[34] Most of the 1IOV conformation was left intact; only residues 199−226 were modeled after 2FB9, corresponding to the lid loop and a buffer region of one or two amino acids on each side of the loop. Ninety comparative models of the open form of DdlB were produced and ranked by their DOPE-HR scores.[33]

Optimization of Starting Structures for Molecular Dynamics. Each starting structure was minimized with the academic version of CHARMM 3.6[21] using SD and ABNR algorithms, explicitly solvated in a rectangular box of 17 832 TIP3 water molecules, neutralized with 25 K^+ and 16 Cl^- ions (to achieve 150 mM K^+, close to the cytosolic concentration), heated to 300 K, and equilibrated for 5 ns using the all-atom CHARMM27 force field[35] and CPT dynamics with the Hoover thermostat, a femtosecond time step, periodic boundary conditions, the SHAKE restraint for bonds involving hydrogen atoms,[36] and the particle mesh Ewald method for electrostatics calculations.[37]

Targeted Molecular Dynamics (TMD) Simulation.[22] 500 ps of TMD simulation was performed with CHARMM 3.6 using explicit solvent. A few MD settings differed from the previous steps: the Leap Verlet integrator and the Berendsen thermostat were used. The TMD-specific parameters INRT, DINC, and FRMS were assigned values 10, 0.00002, and 0.1, respectively. Only protein backbone atoms were selected for the holonomic constraint guiding the TMD simulation.

Off-Path/Replica Path Simulation.[23,24] 314 ps of off-path dynamics simulation was performed on the VRANA-11 parallel computer cluster with CHARMM 3.6 using explicit solvent. Most MD settings were copied from the structure equilibration stage, while the time step was lowered to 0.5 fs. The RPath-specific parameters KRMS, KMAX, and RMAX were assigned values 1000, 500, and 0.5, respectively.

Filtering the Compound Library. The ZINC library of compounds[27] was filtered with the Filter program (OpenEye Scientific Software) with the following choice of descriptors: molecular weight between 100 and 300; 0−2 ring systems; 0−4 H-bond donors; 0−6 H-bond acceptors; 0−5 rotatable bonds, and log *P* between −3.0 and 3.0. Additional filters were employed to eliminate compounds with atoms other than H, C, N, O, F, S, Cl, and Br and compounds with reactive functional groups.

Virtual Screening with FlexX 3.1 (BiosolveIT).[28] The active site was defined as the volume of the enzyme within 8 Å of Arg255 for each structure, and ATP and Mg^{2+} ions were kept in all structures. For the base placement, Triangle Matching was used. This program generated the maxima of 200 solutions per iteration and 200 per fragmentation. All compounds were docked into the active site of each of three conformations of the enzyme and ranked according to the score of the best scored conformation.

Virtual Screening with Fred 2.2.5 (OpenEye Scientific Software).[29] Because of the rigid method of docking implemented in the OpenEye software suite, tautomers and conformers of all compounds were generated beforehand with respective tools Tautomers (with "level" set to 0) and Omega[38] (with "rms" set to 0.8). The receptor sites were prepared with the Fred Receptor tool, with the ATP molecule and Mg^{2+} ions intact in all structures. The active site box was built around Arg255 for each structure. A high quality site shape potential was used to generate the active site contours. The docking was performed with a hit list size of 5 000 000.

Hierarchical Clustering. A hierarchical clustering of the top 10 000 compounds from the consensus score list was performed with the in-house program PyScoreClust. PyScoreClust utilizes the Python extension module PyCluster[39] for clustering and the Indigo/Python module from GGA Software[40] for handling chemical formats and Tanimoto index[41] calculation. Tanimoto index represents similarity between graph-theoretical Indigo molecular fingerprints. The clustering distance between each pair of compounds was defined as 1 − Tanimoto Index. The Euclidean distance metric was employed. The hierarchical tree was generated from a distance matrix formatted as a list of NumPy[42] arrays. The distance between clusters was calculated as the arithmetic mean between cluster centroids. The resulting hierarchical tree was cut to yield an average Tanimoto index of 0.95 or more between each pair of cluster members. From each cluster produced by PyScoreClust a member with the highest consensus score was selected as the representative compound.

Computer Graphics. Figures of protein structures were generated with VMD 1.9.[43] Graphs were drawn with GnuPlot 4.4.[44]

II. Bioactivity Study. *Enzyme Inhibition Assay.* The inhibitory activity of compounds was determined with the colorimetric malachite green assay[45] in which the orthophosphate generated during the reaction was measured. Each compound was tested in duplicate at 500 or 250 μM. Assays were performed at 37 °C in a mixture containing 50 mM HEPES (pH 8.0), 3.25 mM $MgCl_2$, 6.5 mM $(NH_4)_2SO_4$, 700 μM D-Ala, 500 μM ATP, purified DdlB (diluted in 50 mM HEPES (pH 7.2) and 1 mM dithiothreitol), and the test compound. The final volume was 50 μL. All compounds were soluble in the assay mixture containing 5% DMSO. After 20 min of incubation, 100 μL of Biomol reagent was added, and absorbance was read at 650 nm after 5 min. To exclude possible nonspecific (promiscuous) binders, all compounds were tested in the presence of a detergent (Triton X-114, 0.001%).[46] For the best inhibitor the K_i value was determined. This was performed under similar conditions using ATP (500 μM), D-Ala (300, 500, 700, 900, 1100, and 1300 μM), and the inhibitor (200, 300, 400, and 500 μM) with 20 min of incubation at 37 °C. The K_i values were calculated using the Sigma Plot 12 software, where the initial velocity data were fitted to competitive, noncompetitive, and uncompetitive inhibition models.

Compound Analysis. The identities of compounds from Table 1 were analyzed via proton NMR and high resolution mass spectrometry. HPLC was used to verify their purity. HPLC analyses were performed on an Agilent Technologies HP 1100 instrument with a G1365B UV−vis detector (254 nm) using a Luna C18 column (4.6 mm × 250 mm) at a flow rate of 1 mL/min. In method A, the eluent was a mixture of 0.1% TFA in water and methanol; the gradient was from 10% to 90% methanol in 20 min. In method B, the eluent was a mixture of 0.1% TFA in water and acetonitrile; the gradient was from 40% to 90% acetonitrile in 20 min.

*N′-{[(3-Chloroanilino)carbonyl]oxy}isoxazole-5-carboximidamide (**1**, ZINC08536193).* ^{1}H NMR (DMSO-d_6, 400 MHz) δ 7.10−7.12 (m, 2H, Ar-H), 7.24 (bs, 2H, NH_2), 7.35 (t, J = 8.06 Hz, 1H, Ar-H), 7.45−7.47 (m, 1H, Ar-H), 7.68 (t, J = 1.99 Hz, 1H, Ar-H), 8.77 (d, J = 1.88 Hz, 1H, Ar-H), 9.70 (s, 1H, NH). ESI-HRMS m/z calcd for $[M + (H)]^+$ 281.0441, found 281.0438. HPLC method B: 100%, t_R = 6.65 min.

*N′-{[(4-Chloroanilino)carbonyl]oxy}-5-methylisoxazole-3-carboximidamide (**2**, ZINC18142224).* ^{1}H NMR (DMSO-d_6, 400 MHz) δ 2.47 (s, 3H, CH_3), 6.65 (d, J = 0.92 Hz, 1H, Ar-H), 6.95 (bs, 2H, NH_2), 7.37−7.40 (m, 2H, Ar-H), 7.53−7.57 (m, 2H, Ar-H), 9.58 (s, 1H, NH). ESI-HRMS m/z calcd for $[M + (H)]^+$ 295.0598, found 295.0593. HPLC method B: 100%, t_R = 9.08 min.

*4-[(E)-(Isonicotinoylhydrazono)methyl]-6-keto-1H-pyrimidin-2-olate (**3**, ZINC01868219).* ^{1}H NMR (DMSO-d_6, 400 MHz) δ 5.96 (s, 1H, CO-CH-C), 7.82 (d, J = 4.92, 2H, Ar-H), 8.12 (s, 1H, C-CH-N-NH), 8.81 (d, J = 4.83, 2H, Ar-H), 10.76 (bs, 1H, CO-NH-C), 11.21 (s, 1H, N-NH-CO-Ar), 12.58 (bs, 1H, CO-NH-CO). ESI-HRMS m/z calcd for $[M + (H)]^+$ 260.0773, found 260.0784. HPLC method A: 100%, t_R = 7.28 min.

*2,4-Diketo-5-(phenylcarbamoyl)-1H-pyrimidin-6-olate (**4**, ZINC1586033).* ^{1}H NMR (DMSO-d_6, 400 MHz) δ 7.19−7.23 (m, 1H, Ar-H), 7.28−7.42 (m, 2H, Ar-H), 7.52−7.54 (m, 2H, Ar-H), 11.42 (bs, 1H, CO-NH-CO), 11.53 (s, 1H, CO-NH-Ar), 12.03 (bs, 1H, CO-NH-CO), OH exchanged. ESI-HRMS m/z calcd for $[M-(H)]^+$ 246.0515, found 246.0512. HPLC method B: 87.10%, t_R = 3.67 min.

*2-[(7-Methoxy-4-methylquinazolin-2-yl)amino]pyrimidine-4,6-diol (**5**, STK046256).* ^{1}H NMR (DMSO-d_6, 400 MHz) δ 2.84 (s, 3H, CH_3-Ar), 3.98 (s, 3H, CH_3-O), 5.07 (s, 1H, Ar-NH-Ar), 7.16−7.21 (m, 2H, Ar-H), 8.14 (d, J = 8.96 Hz, 1H, Ar-H), 11.29 (bs, 1H, NH), other NH exchanged. ESI-HRMS m/z calcd for $[M + (H)]^+$ 300.1097, found 300.1092. HPLC method B: 100%, t_R = 2.19 min.

*N′-{[(4-Chloroanilino)carbonyl]oxy}pyrazine-2-carboximidamide (**6**, ZINC04351284).* ^{1}H NMR (DMSO-d_6, 400 MHz) δ 7.07 (bs, 2H, NH_2), 7.40 (d, J = 8.93 Hz, 2H, Ar-H), 7.61 (d, J = 8.89 Hz, 2H, Ar-H), 8.74−8.75 (m, 1H, Ar-H), 8.81 (d, J = 2.61 Hz, 1H, Ar-H), 9.40 (d, J = 1.48 Hz, 1H, Ar-H), 9.65 (s, 1H, CO-NH-Ar). ESI-HRMS m/z calcd for $[M + (H)]^+$ 292.0601, found 292.0608. HPLC method B: 100%, t_R = 6.47 min.

*N′-[(2,1,3-Benzothiadiazol-5-ylcarbonyl)oxy]-1,2,4-oxadiazole-3-carboximidamide (**7**, ZINC05092259).* ^{1}H NMR (DMSO-d_6, 400 MHz) δ 7.69 (bs, 2H, NH2), 8.23 (dd, J = 9.09, 0.57 Hz, 1H, Ar-H), 8.36 (dd, J = 9.15, 1.64 Hz, 1H, Ar-H), 9.23 (d, J = 0.62 Hz, 1H, Ar-H), 9.90 (s, 1H, Ar-H). ESI-HRMS m/z calcd for $[M + (H)]^+$ 291.0300, found 291.0298. HPLC method B: 98.73%, t_R = 3.59 min.

■ ASSOCIATED CONTENT

Supporting Information

Similarity search for D-cycloserine analogues; rms distances between consecutive pairs of final RPath conformations; the top-100 list of compounds after clustering; binding modes for seven hit inhibitors. This material is available free of charge via the Internet at http://pubs.acs.org.

■ AUTHOR INFORMATION

Corresponding Author

*For S.G.: phone, +386-1-4769-585; fax, +386-1-4258-031; e-mail, gobecs@ffa.uni-lj.si. For D.J.: phone, +386-1-4760-321; fax, +386-1-4760-300; e-mail, dusa@cmm.ki.si.

Author Contributions

§These authors contributed equally to this work.

Notes

The authors declare no competing financial interest.

■ ACKNOWLEDGMENTS

This work was supported by the European Union FP6 Integrated Project EUR-INTAFAR (Project No. LSHM-CT-2004-512138) under the thematic priority of Life Sciences, Genomics, and Biotechnology for Health. Financial support through Grants P1-0002, P1-0208, L1-4039, and Z1-3666 of the Ministry of Higher Education, Science, and Technology of Slovenia and the Slovenian Research Agency is acknowledged. We thank OpenEye Scientific Software Inc. for free academic licenses of their software, and the Drug Synthesis and Chemistry Branch, Developmental Therapeutics Program, Division of Cancer Treatment and Diagnosis, National Cancer Institute, for supplying compounds for testing. We thank Prof. Dr. Ian Chopra and Dr. Julieanne Bostock for supplying the DdlB enzyme.

■ ABBREVIATIONS USED

ABNR, adopted basis Newton−Raphson; CHARMM, chemistry at Harvard molecular mechanics; CPT, constant pressure/temperature; Ddl, D-alanine:D-alanine ligase; DOPE-HR, discrete optimized protein energy, high resolution; HEPES, 4-(2-hydroxyethyl)-1-piperazineethanesulfonic acid; RA, residual activity; SD, steepest descent; TMD, targeted molecular dynamics

■ REFERENCES

(1) Barreteau, H.; Kovac, A.; Boniface, A.; Sova, M.; Gobec, S.; Blanot, D. Cytoplasmic steps of peptidoglycan biosynthesis. *FEMS Microbiol. Rev.* **2008**, *32*, 168−207.

(2) Walsh, C. T. Enzymes in the D-alanine branch of bacterial-cell wall peptidoglycan assembly. *J. Biol. Chem.* **1989**, *264*, 2393−2396.

(3) Kahan, F. M.; Kahan, J. S.; Cassidy, P. J.; Kropp, H. Mechanism of action of fosfomycin (phosphonomycin). *Ann. N.Y. Acad. Sci.* **1974**, *235*, 364−386.

(4) Vollmer, W.; Blanot, D.; de Pedro, M. A. Peptidoglycan structure and architecture. *FEMS Microbiol. Rev.* **2008**, *32*, 149−167.

(5) Ellsworth, B. A.; Tom, N. J.; Bartlett, P. A. Synthesis and evaluation of inhibitors of bacterial D-alanine:D-alanine ligases. *Chem. Biol.* **1996**, *3*, 37−44.

(6) Neuhaus, F. C.; Lynch, J. L. The enzymatic synthesis of D-alanyl-D-alanine. 3. On the inhibition of D-Alanyl-D-Alanine synthetase by the antibiotic D-cycloserine. *Biochemistry* **1964**, *3*, 471−480.

(7) Lambert, M. P.; Neuhaus, F. C. Mechanism of D-cycloserine action: alanine racemase from *Escherichia coli* W. *J. Bacteriol.* **1972**, *110*, 978−987.

(8) WHO. *Treatment of Tuberculosis: Guidelines*, 4th ed.; World Health Organization: Geneva, Switzerland, 2010; pp 84−85.

(9) Zawadzke, L. E.; Bugg, T. D. H.; Walsh, C. T. Existence of 2 D-alanine-D-alanine ligases in *Escherichia coli*. Cloning and sequencing of the DdlA gene and purification and characterization of the DdlA and DdlB enzymes. *Biochemistry* **1991**, *30*, 1673−1682.

(10) Daub, E.; Zawadzke, L. E.; Botstein, D.; Walsh, C. T. Isolation, cloning, and sequencing of the *Salmonella typhimurium* DdlA gene

with purification and characterization of its product, D-alanine-D-alanine ligase (ADP forming). *Biochemistry* **1988**, *27*, 3701–3708.
(11) Galperin, M. Y.; Koonin, E. V. A diverse superfamily of enzymes with ATP-dependent carboxylate-amine/thiol ligase activity. *Protein Sci.* **1997**, *6*, 2639–2643.
(12) Fan, C.; Park, I. S.; Walsh, C. T.; Knox, J. R. D-Alanine:D-alanine ligase: phosphonate and phosphinate intermediates with wild type and the Y216F mutant. *Biochemistry* **1997**, *36*, 2531–2538.
(13) Shi, Y.; Walsh, C. T. Active-site mapping of *Escherichia coli* D-Ala-D-Ala ligase by structure-based mutagenesis. *Biochemistry* **1995**, *34*, 2768–2776.
(14) Lee, J. H.; Na, Y.; Song, H. E.; Kim, D.; Park, B. H.; Rho, S. H.; Im, Y. J.; Kim, M. K.; Kang, G. B.; Lee, D. S.; Eom, S. H. Crystal structure of the apo form of D-alanine:D-alanine ligase (Ddl) from *Thermus caldophilus*: a basis for the substrate-induced conformational changes. *Proteins* **2006**, *64*, 1078–1082.
(15) Tytgat, I.; Colacino, E.; Tulkens, P. M.; Poupaert, J. H.; Prevost, M.; Van Bambeke, F. DD-Ligases as a potential target for antibiotics: past, present and future. *Curr. Med. Chem.* **2009**, *16*, 2566–2580.
(16) Richards, F. M.; Kundrot, C. E. Identification of structural motifs from protein coordinate data: secondary structure and first-level supersecondary structure. *Proteins* **1988**, *3*, 71–84.
(17) Kitamura, Y.; Ebihara, A.; Agari, Y.; Shinkai, A.; Hirotsu, K.; Kuramitsu, S. Structure of D-alanine-D-alanine ligase from *Thermus thermophilus* HB8: cumulative conformational change and enzyme–ligand interactions. *Acta Crystallogr. D* **2009**, *65*, 1098–1106.
(18) Kovac, A.; Konc, J.; Vehar, B.; Bostock, J. M.; Chopra, I.; Janezic, D.; Gobec, S. Discovery of new inhibitors of D-alanine:D-alanine ligase by structure-based virtual screening. *J. Med. Chem.* **2008**, *51*, 7442–7448.
(19) Vehar, B.; Hrast, M.; Kovac, A.; Konc, J.; Mariner, K.; Chopra, I.; O'Neill, A.; Janezic, D.; Gobec, S. Ellipticines and 9-acridinylamines as inhibitors of D-alanine:D-alanine ligase. *Bioorg. Med. Chem.* **2011**, *19*, 5137–5146.
(20) Guido, R. V.; Oliva, G.; Andricopulo, A. D. Virtual screening and its integration with modern drug design technologies. *Curr. Med. Chem.* **2008**, *15*, 37–46.
(21) Brooks, B. R.; Brooks, C. L., 3rd; Mackerell, A. D., Jr.; Nilsson, L.; Petrella, R. J.; Roux, B.; Won, Y.; Archontis, G.; Bartels, C.; Boresch, S.; Caflisch, A.; Caves, L.; Cui, Q.; Dinner, A. R.; Feig, M.; Fischer, S.; Gao, J.; Hodoscek, M.; Im, W.; Kuczera, K.; Lazaridis, T.; Ma, J.; Ovchinnikov, V.; Paci, E.; Pastor, R. W.; Post, C. B.; Pu, J. Z.; Schaefer, M.; Tidor, B.; Venable, R. M.; Woodcock, H. L.; Wu, X.; Yang, W.; York, D. M.; Karplus, M. CHARMM: the biomolecular simulation program. *J. Comput. Chem.* **2009**, *30*, 1545–1614.
(22) Schlitter, J.; Engels, M.; Kruger, P.; Jacoby, E.; Wollmer, A. Targeted molecular-dynamics simulation of conformational change. Application to the T↔R transition in insulin. *Mol. Simul.* **1993**, *10*, 291–308.
(23) Woodcock, H. L.; Hodoscek, M.; Sherwood, P.; Lee, Y. S.; Schaefer, H. F.; Brooks, B. R. Exploring the quantum mechanical/molecular mechanical replica path method: a pathway optimization of the chorismate to prephenate Claisen rearrangement catalyzed by chorismate mutase. *Theor. Chem. Acc.* **2003**, *109*, 140–148.
(24) Chu, J. W.; Trout, B. L.; Brooks, B. R. A super-linear minimization scheme for the nudged elastic band method. *J. Chem. Phys.* **2003**, *119*, 12708–12717.
(25) Perdih, A.; Solmajer, T. MurD ligase from *Escherichia coli*: C-terminal domain closing motion. *Comput. Theor. Chem.* **2012**, *979*, 73–81.
(26) Czerminski, R.; Elber, R. Reaction-path study of conformational transitions in flexible systems. Applications to peptides. *J. Chem. Phys.* **1990**, *92*, 5580–5601.
(27) Irwin, J. J.; Shoichet, B. K. ZINC: a free database of commercially available compounds for virtual screening. *J. Chem. Inf. Model.* **2005**, *45*, 177–182.
(28) Rarey, M.; Kramer, B.; Lengauer, T.; Klebe, G. A fast flexible docking method using an incremental construction algorithm. *J. Mol. Biol.* **1996**, *261*, 470–489.
(29) Swann, S. L.; Brown, S. P.; Muchmore, S. W.; Patel, H.; Merta, P.; Locklear, J.; Hajduk, P. J. A unified, probabilistic framework for structure- and ligand-based virtual screening. *J. Med. Chem.* **2011**, *54*, 1223–1232.
(30) Kovac, A.; Majce, V.; Lenarsic, R.; Bombek, S.; Bostock, J. M.; Chopra, I.; Polanc, S.; Gobec, S. Diazenedicarboxamides as inhibitors of D-alanine-D-alanine ligase (Ddl). *Bioorg. Med. Chem. Lett.* **2007**, *17*, 2047–2054.
(31) Borstnik, U.; Hodoscek, M.; Janezic, D. Improving the performance of molecular dynamics simulations on parallel clusters. *J. Chem. Inf. Comput. Sci.* **2004**, *44*, 359–364.
(32) Borstnik, U.; Janezic, D. Symplectic molecular dynamics simulations on specially designed parallel computers. *J. Chem. Inf. Model.* **2005**, *45*, 1600–1604.
(33) Eswar, N.; Webb, B.; Marti-Renom, M. A.; Madhusudhan, M. S.; Eramian, D.; Shen, M. Y.; Pieper, U.; Sali, A. Comparative Protein Structure Modeling Using Modeller. In *Current Protocols in Bioinformatics*; Wiley: New York, 2006; Chapter 5, Unit 5.6.
(34) Berman, H. M.; Westbrook, J.; Feng, Z.; Gilliland, G.; Bhat, T. N.; Weissig, H.; Shindyalov, I. N.; Bourne, P. E. The Protein Data Bank. *Nucleic Acids Res.* **2000**, *28*, 235–242 ; www.pdb.org.
(35) Feller, S. E.; MacKerell, A. D. An improved empirical potential energy function for molecular simulations of phospholipids. *J. Phys. Chem. B* **2000**, *104*, 7510–7515.
(36) Ryckaert, J. P.; Ciccotti, G.; Berendsen, H. J. C. Numerical-integration of Cartesian equations of motion of a system with constraints. Molecular-dynamics of *n*-alkanes. *J. Comput. Phys.* **1977**, *23*, 327–341.
(37) Batcho, P. F.; Case, D. A.; Schlick, T. Optimized particle-mesh Ewald/multiple-time step integration for molecular dynamics simulations. *J. Chem. Phys.* **2001**, *115*, 4003–4018.
(38) Hawkins, P. C. D.; Skillman, A. G.; Warren, G. L.; Ellingson, B. A.; Stahl, M. T. Conformer generation with OMEGA: algorithm and validation using high quality structures from the Protein Databank and Cambridge Structural Database. *J. Chem. Inf. Model.* **2010**, *50*, 572–584.
(39) de Hoon, M. J. L.; Imoto, S.; Nolan, J.; Miyano, S. Open source clustering software. *Bioinformatics* **2004**, *20*, 1453–1454.
(40) Pavlov, D.; Rybalkin, M.; Karulin, B.; Kozhevnikov, M.; Savelyev, A.; Churinov, A. Indigo: universal cheminformatics API. *J. Cheminf.* **2011**, *3* (Suppl. 1), P4.
(41) Willett, P.; Barnard, J. M.; Downs, G. M. Chemical similarity searching. *J. Chem. Inf. Comput. Sci.* **1998**, *38*, 983–996.
(42) Oliphant, T. E. Python for scientific computing. *Comput. Sci. Eng.* **2007**, *9*, 10–20.
(43) Humphrey, W.; Dalke, A.; Schulten, K. VMD: visual molecular dynamics. *J. Mol. Graphics* **1996**, *14*, 33–38.
(44) Williams, T.; Keeley, C. Gnuplot 4.4: An Interactive Plotting Program. http://gnuplot.sourceforge.net (accessed Sep 2011).
(45) Walsh, A. W.; Falk, P. J.; Thanassi, J.; Discotto, L.; Pucci, M. J.; Ho, H. T. Comparison of the D-glutamate-adding enzymes from selected gram-positive and gram-negative bacteria. *J. Bacteriol.* **1999**, *181*, 5395–5401.
(46) McGovern, S. L.; Helfand, B. T.; Feng, B.; Shoichet, B. K. A specific mechanism of nonspecific inhibition. *J. Med. Chem.* **2003**, *46*, 4265–4272.